Model Development for Piezoelectric Polymer Unimorphs *

G. Daspit[1], C. Martin[2], J-H. Pyo[3], C. Smith[4], H. To[5]
and
K.M. Furati[6], Z. Ounaies[7], R.C. Smith[8,†]

[1]Department of Mathematics, University of Alabama at Birmingham, Birmingham, AL 35294
[2]Department of Mathematics and Statistics, Texas Tech University, Lubbock, TX 79409
[3]Department of Mathematics, University of Maryland, College Park, MD 20742
[4,8]Center for Research in Scientific Computation, North Carolina State Univ., Raleigh, NC 27695
[5]Department of Mathematics, Temple University, Philadelphia, PA 19122
[6]Department of Mathematical Science, KFUPM, Dhahran 31261, Saudi Arabia
[7]ICASE, NASA Langley Research Center, MS 132C, Hampton, VA 23681

Abstract

This paper addresses the development of distributed models for unimorphs comprised of an active PVDF layer bonded to an inactive polyimide layer. Thin beam theory is employed to quantify displacements along the unimorph length as a function of input voltages. The theory is based on the assumption of linear piezoelectric relations but is posed in a format which can be directly extended to incorporate dielectric hysteresis and nonlinearities if the application warrants. A variety of structural damping models are considered and it is illustrated that in low drive regimes, the assumption of Kelvin-Voigt damping produces a unimorph model which accurately predicts the elliptic losses measured in experimental data.

Keywords: Unimorph model, PVDF, polyimide, piezoelectricity

1. Introduction

Piezoelectric unimorph and bimorph constructions offer unique capabilities for generating large displacements in response to input voltages. The mechanisms which produce these enhanced displacements can be attributed to a number of factors which depend upon the specific configuration under consideration. In all unimorph and bimorph constructions, part of the displacement is due to coupling between an active layer which expands or contracts and an inactive layer which resists deformation. In Rainbow actuators, it has been demonstrated that stress-enhanced domain reorientation contributes to the large observed displacements [9, 11] whereas in THUNDER, the displacements are augmented by the curvature generated by thermal stresses produced during the fabrication of the transducers [6, 8, 22]. In this paper, we focus solely on modeling the interaction between the active and inactive layers, which we term the unimorph mechanism, and direct the reader to the cited reference for details regarding the auxiliary effects in Rainbow and THUNDER.

To date, piezoelectric unimorphs and bimorphs have been comprised primarily of active piezoceramic layers bonded to a variety of metallic or composite inactive layers. A comprehensive review of the history and early applications utilizing bimorphs is provided in [20] and representative unimorph configurations comprised of PZT layers bonded to a variety of metallic layers are illustrated and modeled in [11, 15, 21]. It is noted in these references

*This problem was investigated by the first five authors under the direction of the last three authors during the Industrial Mathematics Modeling Workshop for Graduate Students held at North Carolina State University on July 23-July 31, 2001.

†Corresponding author: rsmith@eos.ncsu.edu, (919) 515-7552

that PZT-based unimorphs and bimorphs have been employed in applications which include pressure and acoustic sensing, precision position control, low-frequency vibration damping and phonograph pickup elements.

The recent genesis of polymer-based unimorph and bimorph designs is motivated by increasingly stringent demands in aeronautic, aerospace and industrial applications coupled with improvements in material design and fabrication. Aeronautic applications, such as flow control on an airfoil, require flexibility, extreme durability, and light weight while aerospace processes often have the additional constraint of robustness with regard to large temperature gradients and high radiation levels. Many of these attributes are provided by recently-developed polyimide compounds. Unimorphs comprised of these materials provide unique control capabilities for high performance processes requiring lightweight, durable, highly robust actuators and sensors.

In this paper we develop a model for a unimorph comprised of an active PVDF layer bonded to an inactive polyimide layer. While PVDF films are not resistant to atomic oxygen, cosmic ray radiation or temperature gradients, this configuration provides a prototype for model development and validation as a step toward the characterization of polyimide structures under current investigation. Low to moderate drive regimes are considered which motivates the assumption of linear piezoelectric relations. Linear beam theory incorporating a variety of structural damping mechanisms is then used to develop a distributed model which quantifies displacements at various points in the unimorph as a function of input voltages. Whereas linear input relations are employed, the formulation is sufficiently general to permit direct extension to incorporate dielectric hysteresis and constitutive nonlinearities if warranted by high drive regimes.

In addition to providing a simulation tool for predicting unimorph displacements as a function of input voltages and forces, the model is amenable to control design and can be directly incorporated in finite element models or software to optimize the performance of systems utilizing polymeric actuators and/or sensors. Finally, it is also sufficiently general to be employed in the analysis and optimization of power requirements for systems utilizing polymeric unimorphs.

The PDE model for the unimorph is developed in Section 2 and a Galerkin method for discretizing the spatial component of the model is summarized in Section 3. The performance of the model is illustrated in Section 4 where it is used to quantify tip displacements as a function of various input voltages.

2. Model Development

For the purposes of model development, we consider the unimorph configuration depicted in Figure 1. The composite is comprised of an active PVDF layer bonded to an inactive polyimide layer which provides both the elastic and adhesive functions. The unimorph is assumed to be fixed at one end and free at the other.

The thickness of the PVDF and polyimide layers are respectively denoted by h_A and h_I with the thickness of the adhesive incorporated in that of the inactive layer. The length and width of the unimorph are respectively denoted by L and b. To establish a coordinate system, the x-axis was taken in the longitudinal direction with $x = 0$ specified at the fixed end of the unimorph. The z-axis was specified in the transverse or normal direction with the material interface taken to be $z = 0$ and the neutral surface denoted by z_{ns}.

The density, Young's modulus and Kelvin-Voigt damping parameters for the active PVDF layer are respectively designated by ρ_A, Y_A and c_A, and ρ_I, Y_I and c_I denote the analogous parameters for the inactive polyimide layer. The electric field and corresponding voltage applied to the PVDF are specified as E and V, the coefficient for air damping is denoted by γ, and distributed normal forces are represented by $f(t, x)$. Finally, transverse displacements are designated by w.

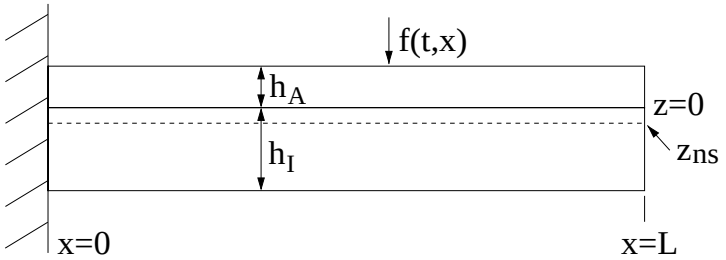

Figure 1. Configuration of the polymer unimorph.

2.1. Constitutive Relations

To designate constitutive relations, we consider low to moderate drive regimes in which linear piezoelectric relations adequately approximate the electromechanical behavior of the material. We also consider both Kelvin-Voigt and viscoelastic models for the material damping.

In the absence of structural damping, it is illustrated in [10] that consideration of the Gibbs free energy for piezoelectric materials yields the linear constitutive relations

$$\begin{aligned} e &= s^E \sigma + dE \\ P &= d\sigma + \kappa^\sigma E \end{aligned} \tag{1}$$

whereas consideration of the elastic Gibbs energy yields

$$\begin{aligned} e &= s^P \sigma + bP \\ E &= -b\sigma + \chi^\sigma P\,. \end{aligned} \tag{2}$$

In both cases, σ and e respectively denote the stress and strain while s^E and s^P are the compliance at constant field and polarization values. Moreover, d, b, κ^σ and χ^σ are piezoelectric and electric coupling coefficients. As discussed in Cady [5], the choice of polarization as an extensive variable in the actuator relation preceded the choice of field and may be more fundamental whereas the field is often employed since it is easily measured. Furthermore, for high drive or high accuracy regimes, the nonlinearities and hysteresis inherent to the field-polarization relation must be incorporated which is facilitated by the polarization-based relation (2). Details regarding the incorporation of the polarization-based hysteresis models developed in [17, 18, 19] in the constitutive relation (2) to provide models for high drive regimes will be reported in a future work.

For the linear regimes under investigation, we consider the actuator relation (1) posed in terms of input voltages and modified to incorporate various models for internal damping. Under the assumption of Kelvin-Voigt damping in both layers, the linear constitutive relation is taken to be

$$\sigma = \begin{cases} Y_A e + c_A \dfrac{de}{dt} - Y_A \dfrac{d_{31}}{h_A} V & , \text{ Active Layer} \\ Y_I e + c_I \dfrac{de}{dt} & , \text{ Inactive Layer.} \end{cases} \tag{3}$$

It is this model which is employed in the unimorph model developed in Section 2.2 and validated with experimental data in Section 4.

Due to the viscoelastic nature of the polymers, a Boltzmann model based on the strain rate history can also be considered. In this case, general constitutive relations are

$$\sigma = \begin{cases} \widetilde{Y}_A e + \displaystyle\int_0^t \widetilde{G}_A(t,s) \frac{de}{ds}(s)\, ds - \widetilde{Y}_A \frac{d_{31}}{h_A} V & , \text{ Active Layer} \\ \widetilde{Y}_I e + \displaystyle\int_0^t \widetilde{G}_I(t,s) \frac{de}{ds}(s)\, ds & , \text{ Inactive Layer} \end{cases} \tag{4}$$

where $\widetilde{G}_A$ and $\widetilde{G}_I$ denote the relaxation moduli for the materials [16]. For the inactive layer, the assumption that $\widetilde{G}_I(t,s) = G_I(t-s)$, where G_I is absolutely continuous (see [7]), yields

$$\begin{aligned} \widetilde{Y}_I e + \int_0^t G_I(t-s) \frac{de}{ds}(s) ds &= \widetilde{Y}_I e(t) + G_I(0) e(t) + \int_0^t \frac{dG_I}{ds}(t-s) e(s)\, ds \\ &= Y_I e(t) + \int_{-r}^0 \frac{dG_I}{ds}(-s) e(t+s)\, ds \end{aligned}$$

where $Y_I \equiv \widetilde{Y}_I + G_I(0)$. To obtain the second equality, it is assumed that $e(t) = 0$ for $t < 0$ and that the material retains a memory for only r units of time. Finally, a common choice for the damping kernel is the exponentially decaying function

$$g_I(s) = \frac{dG_I}{ds}(-s) = \frac{\alpha_I e^{\beta_I s}}{(-s)^{p_I}}\ , \ -r \le s < 0$$

where $\alpha_I, \beta_I > 0$ and $0 \le p_I \le 1$ (see [1, 2, 3]). By employing a similar relation for the active layer, this yields the constitutive relations

$$\sigma = \begin{cases} Y_A e + \displaystyle\int_{-r}^{0} \frac{\alpha_A e^{\beta_A s}}{(-s)^{p_A}} e(t+s)\, ds - Y_A \frac{d_{31}}{h_A} V & , \text{ Active Layer} \\ Y_I e + \displaystyle\int_{-r}^{0} \frac{\alpha_I e^{\beta_I s}}{(-s)^{p_I}} e(t+s)\, ds & , \text{ Inactive Layer} \end{cases} \tag{5}$$

as a model for the viscoelastic behavior of the materials.

2.2. Unimorph Model

For the low drive regimes under consideration, we develop a unimorph model in the context of linear theory based on the following four assumptions: (i) The unimorph thickness is small compared to its length and width, (ii) Deformations are sufficiently small to permit the establishment of kinematic and equilibrium conditions with respect to the unperturbed neutral surface, (iii) Transverse normal stresses are assumed to be negligible and (iv) normal surfaces remain normal during deformation. These assumptions are standard for linear shell, plate or beam theory and were first established by Love [12]. It must be noted that these assumptions will be valid for unimorphs only at low drive levels. Because the active layers generate both in-plane forces and bending moments, assumption (ii) must be relaxed at high drive levels and von Kármán theory based on the balance of forces and moments for a deformed neutral surface must be employed [4, pages 58-60], [13]. The extension of the unimorph models to incorporate the nonlinear coupling between transverse and longitudinal displacements at high drive levels is under investigation.

For assumptions (i) - (iv), the balance of moments and forces yields

$$\begin{aligned} &\rho \frac{\partial^2 w}{\partial t^2} + \gamma \frac{\partial w}{\partial t} + \frac{\partial^2 M}{\partial x^2} = f(t,x) \\ &w(t,0) = \frac{\partial w}{\partial x} = 0 \\ &M(t,L) = \frac{\partial M}{\partial x}(t,L) = 0 \end{aligned} \tag{6}$$

where M denotes the general moments and the composite linear density is

$$\rho = \rho_A h_A b + \rho_I h_I b\,. \tag{7}$$

The boundary conditions reflect the fixed-end condition at $x = 0$ and free-end condition at $x = L$. Formulation (6) provides a strong form of the model quantifying transverse displacements of the unimorph.

To provide a weak form of the model which is appropriate for numerical approximation and subsequent control design, we consider the state space $X = L^2(0, L)$ and space of test functions $V = H_L^2(0, L) = \{\phi \in H^2(0, L) \,|\, \phi(0) = \phi'(0) = 0\}$. The corresponding weak form is then

$$\int_0^L \rho \frac{\partial^2 w}{\partial t^2} \phi \, dx + \int_0^L \gamma \frac{\partial w}{\partial t} \phi \, dx + \int_0^L M \frac{\partial^2 \phi}{\partial x^2} dx = \int_0^L f \phi \, dx \tag{8}$$

which must be satisfied for all $\phi \in V$. It is noted that in the weak form, derivatives are transferred from the moments onto test functions. This reduces smoothness requirements on approximate solutions and eliminates difficulties due to discontinuous input terms.

Since the reference surface for the model is taken to be the neutral surface z_{ns} of the unimorph, the general moments are defined to be

$$M = \int_{-h_I}^{h_A} \sigma(z - z_{ns})\, dz \tag{9}$$

where σ is given by either (3) or (5). To specify z_{ns}, it is noted that at equilibrium, the balance of forces yields

$$\int_0^{h_A} Y_A (z - z_{ns})\, dz + \int_{-h_I}^{0} Y_I (z - z_{ns})\, dz = 0$$

from which it follows that

$$z_{ns} = \frac{Y_A h_A^2 - Y_I h_I^2}{2(Y_A h_A + Y_I h_I)}\,. \tag{10}$$

Analogous neutral surface representations for PZT-based unimorphs are determined in [11, 15].

It is observed that the moment M defined in (9) is comprised of elastic, damping and active components as reflected in the constitutive relations (3) and (5). To indicate this, we express the stress as $\sigma = \sigma_e + \sigma_d + \sigma_{ext}$ with corresponding moment terms defined via (9). Since the strategy in thin beam theory is to represent all forces and moments through the thickness of the structure by resultants at the neutral surface, it is necessary to determine these resultants either directly, in terms of the geometry and properties of the constituent materials, or in terms of effective parameters for the combined structure. The latter approach can incorporate material properties that are known (e.g., stiffness properties) while providing a general framework for the identification of unknown parameters (e.g., damping parameters).

We consider first the moment generated by the elastic component σ_e of the constitutive relation (3). To determine an effective Young's modulus Y for the composite structure, the general moment is equated to the components,

$$\int_{-h_I}^{h_A} bYk(z - z_{ns})^2\,dz = \int_{-h_I}^{0} bY_I k(z - z_{ns})^2\,dz + \int_0^{h_A} bY_A k(z - z_{ns})^2\,dz\,,$$

where k denotes the change in curvature, to yield

$$Y = \frac{Y_I[(h_I + z_{ns})^3 - z_{ns}^3] + Y_A[(h_A - z_{ns})^3 + z_{ns}^3]}{(h_A - z_{ns})^3 + (h_I + z_{ns})^3}\,. \tag{11}$$

For thin beams, $k = -\frac{\partial^2 w}{\partial x^2}$, so the elastic component of the moment is

$$\begin{aligned} M_e &= -\int_{-h_I}^{h_A} bY\frac{\partial^2 w}{\partial x^2}(z - z_{ns})^2\,dz \\ &= YI\frac{\partial^2 w}{\partial x^2} \end{aligned} \tag{12}$$

where

$$I = \frac{b}{3}[(h_A - z_{ns})^3 + (h_I + z_{ns})^3]\,. \tag{13}$$

Through (11) and (13), the effective Young's modulus and generalized moment of inertia for the composite structure can be specified in terms of the geometry and Young's moduli for the constituent materials. Alternatively, the combined parameter YI can be treated as unknown and estimated through a least squares fit to data. In section 4, the accuracy of (11) and (13) is illustrated through comparison with experimental data.

A similar analysis can be employed for the damping component of the moment. However, since values of the damping coefficients for the constituent materials are typically unavailable, we directly consider the moment relation

$$M_d = c_D I\frac{\partial^3 w}{\partial x^2 \partial t} \tag{14}$$

where the parameter $c_D I$ is considered unknown and is determined through inverse problem techniques.

The external moment is given by

$$\begin{aligned} M_{ext} &= \int_0^{h_A} Y_A(z - z_{ns})\frac{d_{31}}{h_A}V(t)\,dz \\ &= k_B V(t) \end{aligned} \tag{15}$$

where

$$k_B = \frac{1}{2}Y_A d_{31}(h_A - 2z_{ns})\,. \tag{16}$$

Noting that $M = M_e + M_d + M_{ext}$, the weak form of the model for the unimorph is then given by

$$\int_0^L \rho\frac{\partial^2 w}{\partial t^2}\phi\,dx + \int_0^L \gamma\frac{\partial w}{\partial t}\phi\,dx + \int_0^L YI\frac{\partial^2 w}{\partial x^2}\frac{d^2\phi}{dx^2}\,dx + \int_0^L c_D I\frac{\partial^3 w}{\partial x^2 \partial t}\frac{d^2\phi}{dx^2}\,dx = \int_0^L f\phi\,dx + \int_0^L k_B V(t)\frac{d^2\phi}{dx^2}\,dx \tag{17}$$

which must be satisfied for all $\phi \in V$. The effective density, Young's modulus, generalized moment of inertia, and external parameter k_B are respectively designated in (7), (11), (13) and (16). An analogous model results if the Kelvin-Voigt damping assumption is replaced by the Boltzmann damping model.

3. Numerical Method

To approximate solutions of the infinite-dimensional model (17), we consider a general Galerkin expansion in the spatial variable to produce a semidiscrete system which can be numerically integrated in time using standard software for initial value problems. The semidiscrete system is also in a form which is amenable for subsequent control design.

The basis $\{\phi_j\}$ is taken to be

$$\phi_1(x) = \widehat{\phi}_0(x) - 2\widehat{\phi}_{-1}(x) - 2\widehat{\phi}_1(x)$$
$$\phi_j(x) = \widehat{\phi}_j(x) \quad , \quad j = 2, \cdots, N+1$$

where $\widehat{\phi}_j$ are canonical cubic B-splines defined by

$$\widehat{\phi}_j(x) = \frac{1}{h^3} \begin{cases} (x - x_{j-2})^3 & , \ x \in [x_{j-2}, x_{j-1}) \\ h^3 + 3h^2(x - x_{j-1}) + 3h(x - x_{j-1})^2 - 3(x - x_{j-1})^3 & , \ x \in [x_{j-1}, x_j) \\ h^3 + 3h^2(x_{j+1} - x) + 3h(x_{j+1} - x)^2 - 3(x_{j+1} - x)^3 & , \ x \in [x_j, x_{j+1}) \\ (x_{j+2} - x)^3 & , \ x \in [x_{j+1}, x_{j+2}) \\ 0 & , \ \text{otherwise} \end{cases}$$

where $h = L/N$ (see [14]). Due to the modification of ϕ_1, elements in the approximating subspace $H^N(0, L) = \text{span}\{\phi_j\}$ satisfy the fixed-end condition at $x = 0$. Hence approximate solutions

$$w^N(t, x) = \sum_{j=1}^{N+1} w_j(t)\phi_j(x) \tag{18}$$

satisfy the essential boundary conditions $w^N(t, 0) = \frac{\partial w^N}{\partial x}(t, 0)$ while inherently satisfying the natural boundary condition at $x = L$ due to the weak formulation of the problem.

To obtain a semidiscrete system, the infinite-dimensional system (17) is projected into $H^N(0, L) \subset V = H^2_L(0, L)$ to yield the vector-valued system

$$M\ddot{\vec{w}}(t) + C\dot{\vec{w}}(t) + K\vec{w}(t) = \vec{f}(t) + \vec{b}V(t)$$

where $\vec{w}(t) = [w_1(t), \cdots, w_{N+1}(t)]^T$ and

$$[M]_{ij} = \rho \int_0^L \phi_i \phi_j \, dx \qquad [\vec{f}]_i = \int_0^L f\phi_i \, dx$$

$$[K]_{ij} = YI \int_0^L \phi_i'' \phi_j'' \, dx \qquad [\vec{b}]_i = k_B \int_0^L \phi_i'' \, dx$$

$$[C]_{ij} = \gamma \int_0^L \phi_i \phi_j \, dx + c_D I \int_0^L \phi_i'' \phi_j'' \, dx \, .$$

The equivalent first-order system is

$$\dot{y}(t) = Ay(t) + BV(t) + F(t) \tag{19}$$

where

$$A = \begin{bmatrix} 0 & I \\ -M^{-1}K & -M^{-1}C \end{bmatrix} \quad , \quad B = \begin{bmatrix} 0 \\ M^{-1}\vec{b} \end{bmatrix} \quad , \quad F = \begin{bmatrix} 0 \\ M^{-1}\vec{f} \end{bmatrix}$$

and $y(t) = [\vec{w}(t), \dot{\vec{w}}(t)]^T = [w_1(t), \cdots, w_{N+1}(t), \dot{w}_1, \cdots, \dot{w}_{N+1}(t)]^T$. The system (19) is in a form which is amenable to forward simulations, parameter estimation and linear control design.

4. Experimental Model Validation

To illustrate low drive attributes of the model, we consider the characterization and prediction of displacements generated by a polymer unimorph having the dimensions and material properties compiled in Table 1. Displacements generated in response to 1 Hz peak input voltages of 25 V, 50 V, 75 V and 100 V were measured at the tip of the unimorph and are plotted in Figure 2. The corresponding peak-to-peak unimorph responses are plotted in Figure 3 along with a linear fit to the data. Both the dynamic responses and peak-to-peak values indicate that within the considered drive regime, the unimorph dynamics are approximately linear so a linear model is appropriate. Furthermore, the 50 V through 100 V data in Figure 2 indicate the level energy loss which must be characterized by the model at higher drive levels.

To employ the previously developed model, geometric and material parameters must be determined for the specific unimorph under consideration. It is noted that accurate values for geometric parameters can be obtained through measurements (e.g., h_I, h_A, L, b) whereas initial estimates for certain material parameters (e.g., ρ_A, ρ_I, Y_A, Y_I) can be obtained from manufacturer specifications or auxiliary experiments. Other parameters, such as the damping coefficients γ and $c_D I$ are typically unknown and must be estimated through a least squares fit to data.

Parameters estimated through a least squares fit to the 100 V data are summarized in Table 1 along with experimentally determined ranges for the parameters when the latter were available. For the coefficient d_{31}, the range was determined by considering a 20% measurement error about a mean value of 25×10^{-12} C/N. It is noted that all model parameters lie within the experimental range.

The model fit to the 100 V data and model predictions, obtained with the same parameter values at 25 V, 50 V and 75 V are compared with corresponding experimental data in Figures 2 and 3. It is observed that throughout the considered drive range, the model provides accurate predictions of both the unimorph displacements and the energy losses measured at the higher drive levels.

We point out that the model predictions in Figures 2 and 3 were obtained using the Kelvin-Voigt internal damping model quantified in the constitutive relation (3). While this provides an accurate characterization of measured energy losses, the resulting damping parameter $c_D I = 2.2848 \times 10^{-7}$ is only two orders of magnitude smaller than the stiffness parameter $YI = 1.7250 \times 10^{-5}$. This is significantly larger than damping values estimated for elastic materials which are often five orders of magnitude less than corresponding stiffness parameters (see pages 134, 147 of [4]). The relatively large damping coefficients probably reflect the viscoelastic nature of the polymers which indicates that Boltzmann damping models of the type employed in the constitutive relations (4) or (5) may provide a more comprehensive technique for quantifying the damping observed in polymer unimorphs throughout extended drive regimes. The numerical approximation and validation of the unimorph model with Boltzmann damping is under current investigation.

Symbol	Units	Experimental Range	Employed in Model	Meaning
L	m	0.03	0.03	Unimorph length
b	m	0.013	0.013	Unimorph width
h_A	m	52×10^{-6}	52×10^{-6}	Thickness of active layer
h_I	m	125×10^{-6}	137×10^{-6}	Thickness of inactive layer
ρ_A	kg/m^3	1.78×10^{3}	1.78×10^{3}	Density of active layer
ρ_I	kg/m^3	1.3×10^{3}	1.3×10^{3}	Density of inactive layer
Y_A	N/m^2	$2.0\times10^{9} - 2.6\times10^{9}$	2.0×10^{9}	Young's modulus of active layer
Y_I	N/m^2	$2.5\times10^{9} - 2.8\times10^{9}$	2.7×10^{9}	Young's modulus of inactive layer
c_D	Nsec/m^2		2.2848×10^{-7}	Coefficient of structural dampening
γ	Nsec/m^2		0.005	Coefficient of air dampening
d_{31}	C/N	$20\times10^{-12} - 27\times10^{-12}$	20×10^{-12}	Piezoelectric coefficient

Table 1. Parameters employed in the model along with experimental ranges for the parameters.

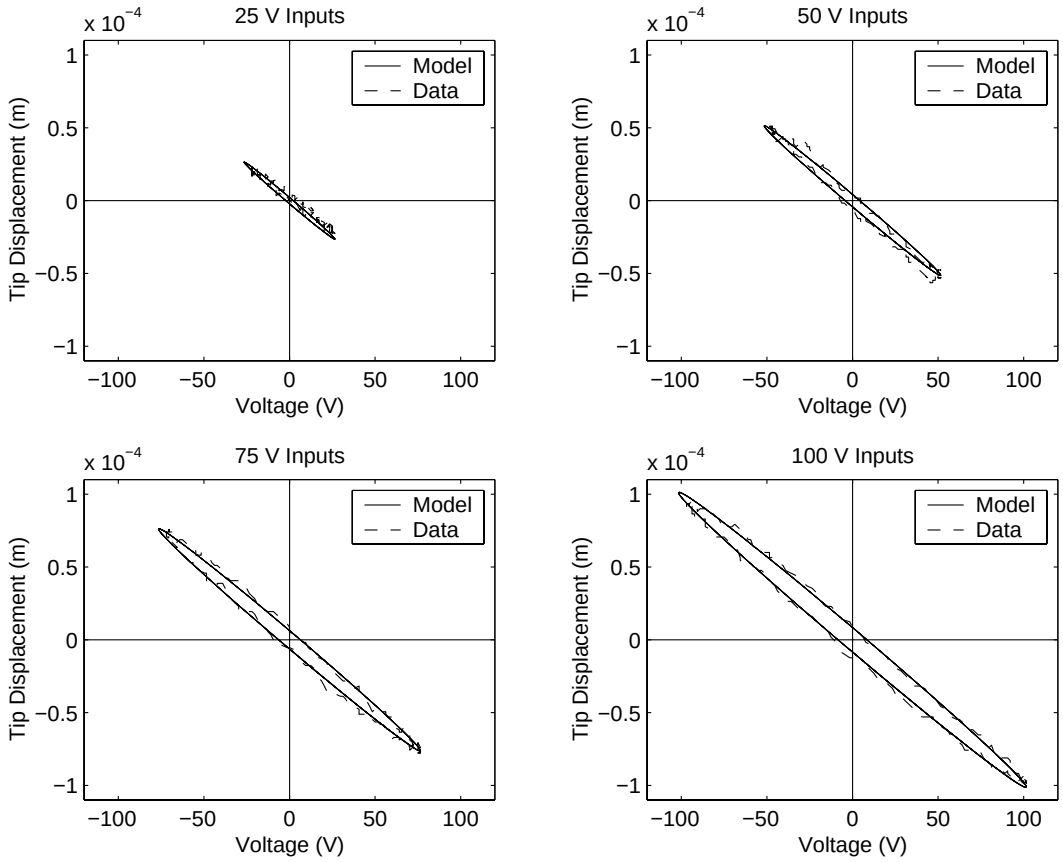

Figure 2. Experimental data, model fit at 100 V and model predictions at 25 V, 50 V and 75 V.

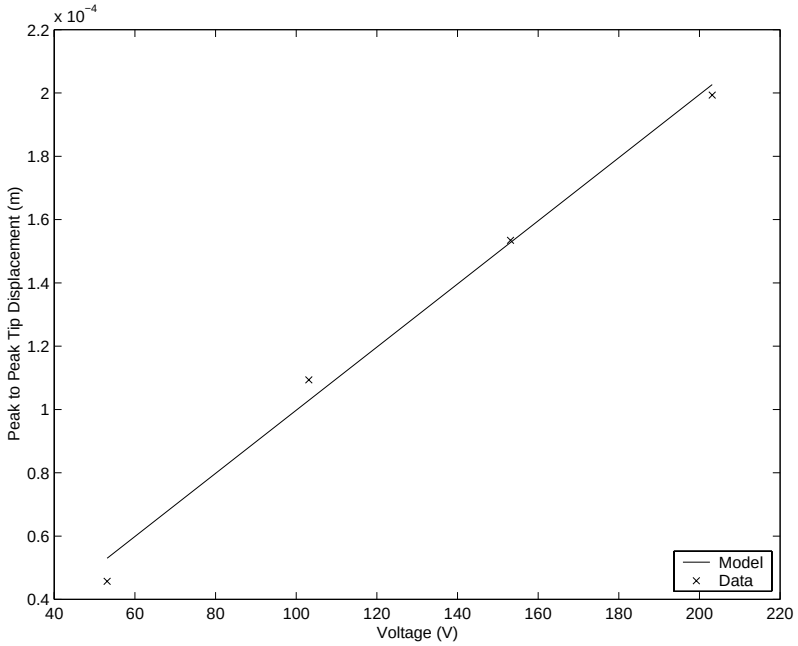

Figure 3. Peak-to-peak experimental data and model predictions.

For the drive levels and frequency ranges under consideration, we note that the losses observed in the data were accurately quantified by considering them to be due to structural damping rather than dielectric loss mechanism. Because electromechanical effects are fully coupled in dynamic applications, it appears difficult to isolate dielectric mechanisms from purely structural damping. It is hypothesized that observed loss mechanisms are quite often due to both phenomena and we are currently designing experiments to isolate the individual effects at both low drive levels where structural damping appears to dominate and high drive regimes where dielectric losses due to domain rotation and domain wall effects become prominent.

5. Concluding Remarks

The thin beam model presented here provides an initial characterization of polymer unimorphs operating at low to moderate drive levels. It was observed that the model accurately predicted both the unimorph dynamics and peak-to-peak displacements for the considered drive regimes. As noted throughout the model development, however, a number of extension are required to achieve a modeling methodology which is accurate for the high drive regimes anticipated for current and future high performance applications.

The primary extensions are motivated by the hysteresis and constitutive nonlinearities inherent to the materials, the development of nonlinear displacement models, and the development of damping models commensurate with the viscoelastic nature of the polymers. As discussed in Section 2, hysteresis models for ferroelectric and piezoelectric materials have been developed [17, 18, 19] and can be directly incorporated in constitutive relations. The inclusion of these constitutive relations in the unimorph model and subsequent experimental validation are under investigation. At high drive levels, it is also anticipated that nonlinear von Kármán relations may be required to accurately quantify large displacements. As detailed in [4, 13], these relations employ the deformed neutral surface in kinematic and equilibrium conditions which will incorporate the inherent coupling between longitudinal and transverse displacements. Finally, it is anticipated that the Boltzmann relations considered in (5) will provide a more comprehensive damping model for these viscoelastic materials. The numerical approximation of the Boltzmann model and experimental validation are under investigation.

A deeper issue which transcends polymer unimorphs concerns the nature of energy losses observed in ferroelectric and piezoelectric materials at low drive levels. For dynamic responses in which losses are elliptic and devoid of a cusp at field or voltage reversal, it is hypothesized that losses are due to both structural damping and dielectric losses which are fully coupled and hence difficult to differentiate in measurements. This is contrasted with dielectric behavior at higher drive levels in which a reversal in the input produces a distinct reversal in the output due to domain switching and relaxation of domain walls. The design of experiments to discern between dielectric losses and structural damping in piezoelectric and general ferroelectric materials is under investigation.

Acknowledgements

The research of R.C.S. was supported in part through the NASA grant NAG-1-01041 and in part by the Air Force Office of Scientific Research under the grant AFOSR-F49620-01-1-0107. The Industrial Mathematics Modeling Workshop was supported by the National Science Foundation through the grant DMS-0098783 with additional supported provided by the Center for Research in Scientific Computation and the Department of Mathematics, North Carolina State University.

References

[1] H.T. Banks, R.H. Fabiano and Y. Wang, "Estimation of Bolzmann damping coefficients in beam models," Proceedings of COMCON Workshop on Stabilization of Flexible Structures, A.V. Balakrishnan and J.P. Zolesio, eds., Optimization Software Inc., New York, pp. 13-35, 1987.

[2] H.T. Banks, R.H. Fabiano and Y. Wang, "Inverse problem techniques for beams with tip body and time hysteresis damping," *Matemática Aplicada e Computacional*, 8(2), pp. 101-118, 1989.

[3] H.T. Banks, N.G. Medhin and Y. Zhang, "A mathematical framework for curved active constrained layer structures: Well-posedness and approximation," *Num. Func. Anal. and Opt.*, 17, pp. 1-22, 1996.

[4] H.T. Banks, R.C. Smith and Y. Wang, *Smart Material Structures: Modeling, Estimation and Control*, Masson/John Wiley, Paris/Chichester, 1996.

[5] W.G. Cady, *Piezoelectricity*, McGraw-Hill, New York, 1946.

[6] M. Capozzoli, J. Gopalakrishnan, K. Hogan, J. Massad, T. Tokarchik, S. Wilmarth, H.T. Banks, K.M. Mossi and R.C. Smith, "Modeling aspects concerning THUNDER actuators," Proceedings of the SPIE, Smart Structures and Materials 1999, Volume 3667, pp. 719-727, 1999.

[7] R.M. Christensen, *Theory of Viscoelasticity, An Introduction*, Academic Press, New York, 1982.

[8] M.W. Hyer and A. Jilani, "Predicting the deformation characteristics of rectangular unsymmetrically laminated piezoelectric materials," *Smart Materials and Structures*, 7, pp. 1-8, 1998.

[9] G. Li, E. Furman and G.H. Haertling, "Stress-enhanced displacements in PLZT Rainbow actuators," *J. Am. Ceram. Soc.,* 80(6), pp. 1382-1388, 1997.

[10] T. Ikeda, *Fundamentals of Piezoelectricity*, Oxford University Press, Oxford, 1990.

[11] X. Li, W.Y. Shih, I.A. Aksay and W.-H. Shih, "Electromechanical behavior of PZT-brass unimorphs," *J. Am. Ceram. Soc.,* 82(7), pp. 1733-1740, 1999.

[12] A.E.H. Love, *A Treatise on the Mathematical Theory of Elasticity*, Cambridge University Press, Fourth Edition, 1927.

[13] A.W. Leissa, *Vibration of Plates*, NASA SP-160, 1969, Reprinted by the Acoustical Society of America through the American Institute of Physics, 1993.

[14] P.M. Prenter, *Splines and Variational Methods*, Wiley, New York, 1975.

[15] W.P. Robbins and D.E. Glumac, "A planar unimorph-based actuator with large vertical displacement capability. Part II: Theory," *IEEE Transactions on Ultrasonics, Ferroelectrics and Frequency Control,* 45(5), pp. 1151-1159, 1998.

[16] I.H. Shames and F.A. Cozzarelli, *Elastic and Inelastic Stress Analysis*, Taylor and Francis, Washington, DC, 1997.

[17] R.C. Smith and C.L. Hom, "Domain wall theory for ferroelectric hysteresis," *Journal of Intelligent Material Systems and Structures*, 10(3), 1999, pp. 195-213.

[18] R.C. Smith and Z. Ounaies, "A domain wall model for hysteresis in piezoelectric materials," *Journal of Intelligent Material Systems and Structures*, 11(1), 2000, pp. 62-79.

[19] R.C. Smith and Z. Ounaies, "A model for asymmetric hysteresis in piezoceramic materials," in *Materials for Smart Systems III*, Material Research Society Symposium Proceedings Volume 604, 2000, pp. 285-290.

[20] J.G. Smits, S.I. Dalke and T.K. Cooney, "The constituent equations of piezoelectric bimorphs," *Sensors and Actuators A*, 28, pp. 41-61, 1991.

[21] Q.-M. Wang, X.-H. Du, B. Xu and L.E. Cross, "Electromechanical coupling and output efficiency of piezoelectric bending actuators," *IEEE Transactions on Ultrasonics, Ferroelectrics and Frequency Control,* 46(3), pp. 638-646, 1999.

[22] Wieman, R.C. Smith, T. Kackley, Z. Ounaies and J. Bernd, "Displacement Models for THUNDER Actuators Having General Loads and Boundary Conditions," Proceedings of the SPIE, Smart Structures and Materials 2001, Volume 4326, pp 252-263, 2001.